

## Article

# Petrogenesis and Geodynamic Significance of the Early Triassic Nanpo Adakitic Pluton of the Luang Prabang-Loei Tectonic Belt (Northwestern Laos) in the East Tethys Domain: Constraints from Zircon U-Pb-Hf Isotope Analyses and Whole-Rock Geochemistry

Hui Li <sup>1</sup> , Jie Gan <sup>2,3,\*</sup>, Zhengwei He <sup>1</sup>, Yu Gan <sup>4</sup>, Bin Wang <sup>1,4</sup>, Yong Li <sup>4</sup> and Wei Jiang <sup>4</sup>

<sup>1</sup> College of Earth Science, Chengdu University of Technology, Chengdu 610059, China; lihui@stu.cdut.edu.cn (H.L.); hzw@cdut.edu.cn (Z.H.); wangbin3088@163.com (B.W.)

<sup>2</sup> College of Geophysical, Chengdu University of Technology, Chengdu 610059, China

<sup>3</sup> Geological Resources and Geological Engineering Postdoctoral Workstation, Chengdu University of Technology, Chengdu 610059, China

<sup>4</sup> The 7th Geological Team of the Bureau of Geological and Mineral Resources of Sichuan, Leshan 614000, China; 13990657092@163.com (Y.G.); lyuyun515@163.com (Y.L.); 13890618175@163.com (W.J.)

\* Correspondence: ganjie@cdut.edu.cn

**Abstract:** Adakites are magmatic rocks with specific geochemical characteristics and specific dynamics that provide important clues to understanding the magmatic-tectonic evolution of orogenic belts. We studied the Early Triassic Nanpo adakitic pluton of the Luang Prabang-Loei tectonic belt in the Eastern Tethys domain (Laos Sarakan) using detailed petrological, zircon U-Pb chronological, whole-rock geochemical, and zircon Lu-Hf isotope studies to constrain their petrogenesis. The rocks are predominantly diorites and granodiorites with Early Triassic zircon U-Pb emplacement ages ranging from  $247.9 \pm 1.0$  to  $249.0 \pm 2.4$  Ma. Moderate SiO<sub>2</sub> (56.26–65.95 wt%) and Na<sub>2</sub>O (3.24–5.00 wt%) contents, with Na<sub>2</sub>O/K<sub>2</sub>O values between 1.76 and 2.51 and A/CNK values between 0.81 and 0.94, indicate that the rocks belong to the metaluminous calc-alkaline rock series. The high Sr content (590–918 ppm), low Y (6.30–11.89 ppm) and Yb (1.99–3.44 ppm) contents, intermediate Mg# (42–50) values, and high Sr/Y and (La/Yb)<sub>N</sub> ratios (Sr/Y = 24–41, (La/Yb)<sub>N</sub> = 6.84–13.8) are typical for adakites. Zircon Hf isotope analysis shows a significant variation in the εHf(t) values (6.7–12.0), with a mean value of 9.4 and a T<sub>DM2</sub> of 512–845 Ma. Geochemical evidence indicates that the Nanpo adakitic rock was formed by the partial melting of the thickened lower crust in the plate-breaking environment and has an important contribution to the underplated mantle-derived magma. We propose that the Early Triassic adakites in the Luang Prabang-Loei tectonic belt formed during the transition from subduction to a continental collision, and the mixing of crust- and mantle-derived magmas is the main mechanism for the growth of continental crust in the Paleo-Tethys orogenic belt of southeastern Asia.

**Keywords:** adakite; magmatism; tectonic evolution; Paleo-Tethys; Luang Prabang-Loei structural belt



**Citation:** Li, H.; Gan, J.; He, Z.; Gan, Y.; Wang, B.; Li, Y.; Jiang, W. Petrogenesis and Geodynamic Significance of the Early Triassic Nanpo Adakitic Pluton of the Luang Prabang-Loei Tectonic Belt (Northwestern Laos) in the East Tethys Domain: Constraints from Zircon U-Pb-Hf Isotope Analyses and Whole-Rock Geochemistry. *Minerals* **2023**, *13*, 821. <https://doi.org/10.3390/min13060821>

Academic Editor: Sung Hi Choi

Received: 2 May 2023

Revised: 15 June 2023

Accepted: 15 June 2023

Published: 16 June 2023



**Copyright:** © 2023 by the authors. Licensee MDPI, Basel, Switzerland. This article is an open access article distributed under the terms and conditions of the Creative Commons Attribution (CC BY) license (<https://creativecommons.org/licenses/by/4.0/>).

## 1. Introduction

The Indochina Massif is a major component of the East Tethys domain and records multiple phases of convergence between the Tethys and Asia [1–4]. Therefore, the massif is an ideal laboratory for studying the dynamics of subduction-extinction of the Tethys Ocean [5,6]. The Luang Prabang-Loei tectonic belt is located at the northwestern margin of the Indochina massif and represents a southward extension of the Sanjiang Tethys tectonic domain in southwestern China. The belt comprises a large number of Permian-Triassic intermediate volcanic rocks, volcanoclastic rocks, and other co-magmatic rocks that were

formed during the evolution of the ancient Tethys Ocean, thus constituting a huge magmatic arc belt [7–10]. The Luang Prabang-Loei magmatic arc belt not only records the subduction of the Paleo-Tethys oceanic crust and the subsequent co-collisional and post-collisional extension processes but also enables us to reveal the crustal growth of the Paleo-Tethys orogenic belt, thus providing insight into orogenic processes in southeastern Asia [11–13]. However, the lack of detailed geological studies has led to an ongoing controversy about the tectonic-magmatic evolution of this orogenic belt [14–17]. For instance, Late Permian island-arc magmatism recognized within the Luang Prabang-Loei tectonic belt has been attributed to the subduction of the Sibumasu massif to the Indochina plate during the closure of the Southeast Asian Paleo-Tethys Ocean in the Middle Triassic [18,19]. In other models, the subduction of the Southeast Asian Paleo-Tethys Ocean continued until the Late Triassic or Late Cenozoic [20,21]. In most studies, it is proposed that the Paleo-Tethys Ocean in Southeast Asia was closed in the late Permian and that the Late Permian-Triassic granitoids were formed in a post-collisional setting [22–25].

Adakites or adakitic rocks are igneous rocks that form in volcanic arc environments by the melting of young ( $\leq 25$  Ma) subducted oceanic crust [26]. In recent years, the understanding of adakites has made major progress [27,28]. Based on the geochemical characteristics of plutonic adakitic rocks and the inferred crystallization conditions, it is recognized that their formation is related to the growth of the continental crust [28]. Moreover, adakites may provide information on the lithospheric structure and magmatic evolution of subduction zones [29,30]. Adakite can be formed by the partial melting of the subducted oceanic plate [26,31], the partial melting of the thickened lower crust of a basaltic composition [32–34], the partial melting of the delaminated lower crust [17], or the crystallization and differentiation of basaltic magma or mixing with acidic magma [35]. Therefore, identifying the genetic types of adakitic rocks, in combination with the detection of their emplacement age and the tectonic environment that prevailed during the emplacement, is the key to revealing the tectonic evolution and crustal growth mechanism of orogenic belts [26,36].

Because of the high closure temperature ( $>900$  °C) of the zircon Lu-Hf isotopic system and the fact that the Lu-Hf isotopic system, in contrast to the Sm-Nd isotopic system, is almost unaffected by mineral inclusions [37], zircon can maintain the original Hf isotopic composition of the source region, even in cases of later high-grade metamorphic overprint [38]. Therefore, Hf isotope studies have been conducted to constrain various geological processes, including rock genesis and source area identification, mantle composition and evolution, regional tectonic evolution, magmatism, and metamorphism [39]. We conducted systematic petrological, zircon U-Pb chronological, whole-rock geochemical, and zircon Lu-Hf isotopic analyses on the Triassic adakites of the Luang Prabang-Loei tectonic belt (northwestern Laos) to reconstruct the tectono-magmatic evolution of the Southeast Asian Paleo-Tethys orogenic belt.

Previous studies have mainly focused on the Late Permian–Middle Triassic island arc magmatism or individual ore deposits of the region [40]. The presence of adakites in northwestern Laos has not been reported so far. Therefore, the petrogenesis and tectonic setting of the Early Triassic adakites in the Luang Prabang-Loei tectonic belt were uncertain [41]. The results of our study provide new insight into the understanding of the tectono-magmatic interaction during the evolution of the Paleo-Tethys in Southeast Asia. Thus, the adakites provide new data for the Paleo-Tethys orogeny and crustal growth processes at the northwestern margin of the Indochina Massif.

## 2. Regional Geological Background

The Luang Prabang-Loei tectonic belt is located in the northern part of the Southeast Asia region [42]. The belt spreads in a north-east to south-west direction, with a north-south length of about 800 km and an east-west width of about 200 km (Figure 1). The Dien Bien Phu-Loei suture zone and the Nam-Uttaradit suture zone mark the eastern and western boundaries of the belt, respectively, and represent remnants of the Paleo-Tethys Ocean [11].

The Simao Block of Sanjiang in southwest China constitutes the northern boundary, and the Meiping Fault is the southern limit [11–13]. The Luang Prabang-Loei tectonic belt is divided by the Pak Lay deep major fault into the Simao-Phitsanulok basin and the Mojiang-Loei volcanic arc belt. The Luang Prabang-Loei tectonic belt is part of the eastern section of the Paleo-Tethys tectonic domain and is linked with the western Pacific tectonic domain to the south [43]. Although the Luang Prabang-Loei tectonic belt has undergone many phases of magmatic activity and also records multiple tectonic-magmatic stages, earlier research has found only scant evidence of magmatic activity connected to the closing of the Paleo-Tethys Ocean [44]. Therefore, the understanding of the tectono-magmatic evolution associated with this process is poor. A large number of Late Permian-Triassic magmatic rocks and numerous polymetallic deposits, including shallow-formed hydrothermal gold, porphyry copper-gold, and siliciclastic copper-gold ores, developed during the Paleo-Tethys orogeny [24,25], making the Luang Prabang-Loei tectonic belt one of the most important polymetallic resources in Southeast Asia. Therefore, studying the petrogenesis of the Early Triassic igneous rocks not only contributes to a better understanding of the tectono-magmatic evolution but also helps in deciphering the metallogenic background of the study area.

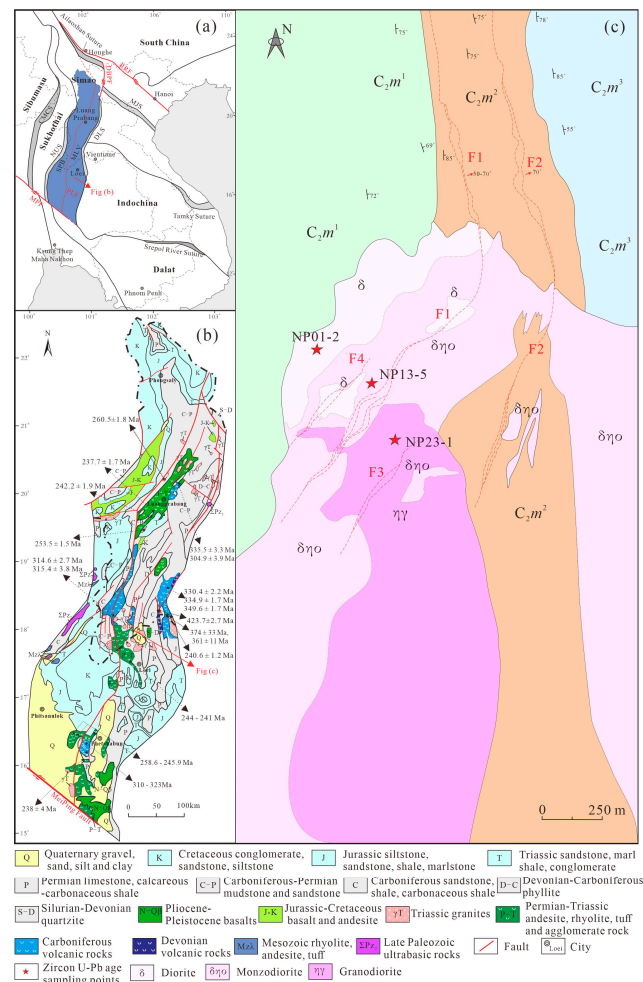


**Figure 1.** Division of tectonic units in Southeast Asia (a); Geological map of Luang Prabang-Loei metallogenic belt (b) (modified from [11–13]); Geological map of Nanpo adakite rock mass (c). RRF—Red River Fault, DBPF—Dien Bien Phu Fault, NUS—Nan Uttaradit Suture, MJSZ—Majiang Suture, DLS—Dien Bien Phu-Loei Suture, MPF—Meiping Fault, CMCS—Changning-Menglian-Chiengmai Suture, SPB—Simao-Phitsanulok Basin, MLV—Mojiang-Loei Volcanic, PLF—Pak Lay Fault.

### 3. Sample and Petrographic Characteristics

The Nanpo Complex is an intrusive magmatic body composed of intermediate plutonic rocks that is located in the south-central section of the Luang Prabang-Loei tectonic belt, close to the Sarakan area of northwestern Laos. The magmatic complex is mainly composed of diorite and intrudes into the Upper Carboniferous Mengnan County Formation ( $C_2m$ ). The body can be subdivided into three gradual transitional lithologic zones: diorite in the marginal zone, monzodiorite in the transitional zone, and granodiorite in the central zone (Figure 2).

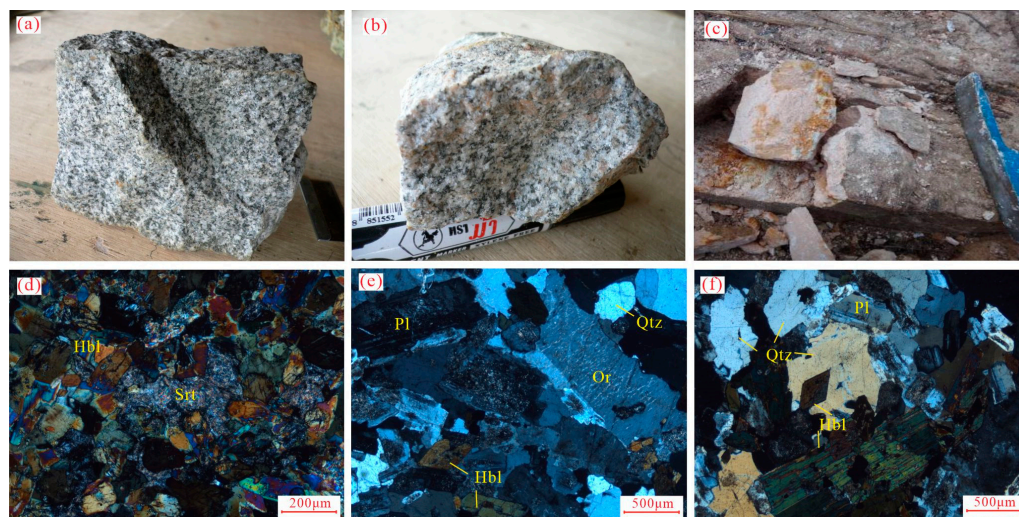


**Figure 2.** Hand specimens and photomicrographs of the Nanpo magmatic rocks: (a,d) diorite; (b,e) monzodiorite; (c,f) granodiorite. Abbreviations: Hbl, Hornblende; Pl, plagioclase; Or, orthoclase; Qtz, quartz; Srt, sericite.

The fine- to medium-grained and massive diorites show a dark brown weathering surface, whereas the fresh surface is gray. The mineral composition is dominated by plagioclase (65%), minor hornblende (15%) and quartz (5%), orthoclase (5%), biotite (3%), diopside (3%), as well as zircon, apatite, sphene, and other accessory minerals. The medium-grained and massive monzodiorites show a black–brown weathering surface, whereas the fresh surface is gray–white to light gray. The mineral composition is dominated by plagioclase (55%), orthoclase (15%), quartz (10%), hornblende (10%), and moderate amounts of biotite (4%), diopside (3%), and accessory zircon, apatite, and titanite. The fine- to medium-grained and massive granodiorites exhibit yellowish-brown weathering surfaces and grayish-white to light gray fresh surfaces. They are composed of plagioclase (45%), quartz (20%), and orthoclase (15%), with minor biotite (5%), hornblende (10%), and accessory zircon and apatite.

A total of 15 representative rock samples were collected for geochemical studies; three samples, i.e., the diorite (sample NP01-2), monzodiorite (sample NP13-5), and granodiorite (sample NP23-1), were selected for zircon U-Pb and Lu-Hf isotope analysis. Zircons show clean surfaces and are commonly colorless and transparent. Most grains form euhedral to semi-euhedral elongated columns. A few zircons are spherical grains. The sizes mostly range between 100 and 200  $\mu\text{m}$ . The length of some individual crystals reaches 230  $\mu\text{m}$ . The aspect ratios vary between 1.5 and 2.5. CL images reveal oscillatory zoning (Figure 3), which is typical for magmatic zircons.

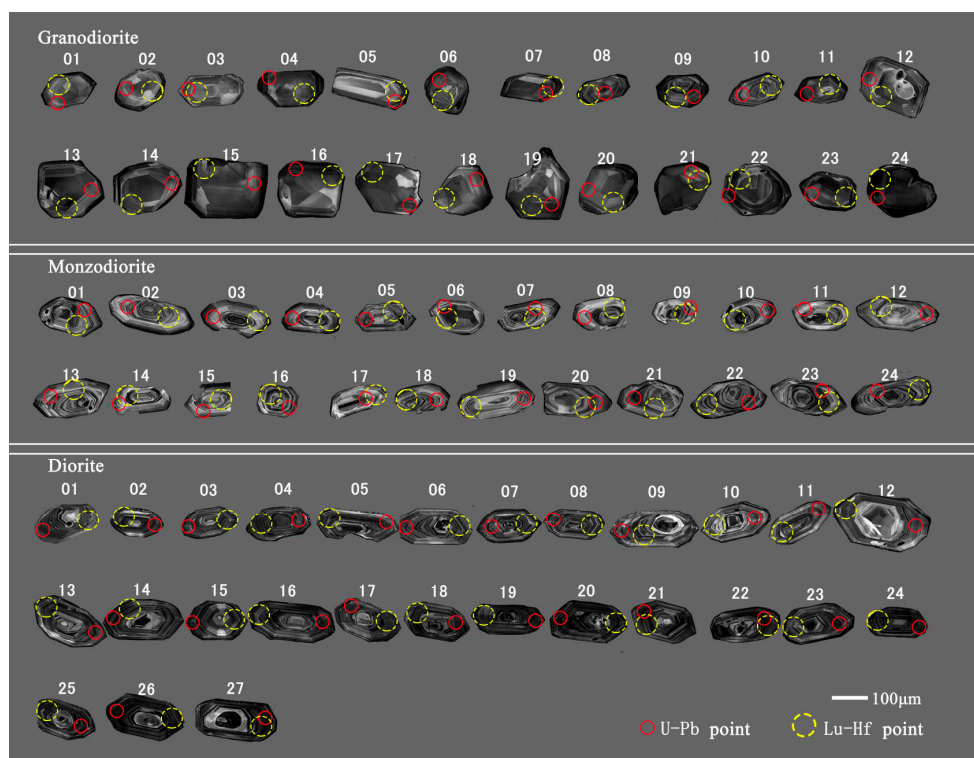


**Figure 3.** CL images of zircons from the Nanpo diorite pluton.

#### 4. Analytical Methods

##### 4.1. Whole-Rock Geochemistry

The whole-rock major, trace, and rare earth elements were analyzed at Chengdu Pupu Testing Technology Co. The rock samples were coarsely crushed to the centimeter level, and fresh sample material without alteration and vein penetration was selected. The material was washed with purified water, dried, and crushed to a powder below 200 mesh for further analysis. For the major element analysis, the powdered samples were weighed, mixed with  $\text{Li}_2\text{B}_4\text{O}_7$  (1:8), and heated to  $1150\text{ }^\circ\text{C}$  to obtain a glass sheet in a platinum crucible. Subsequently, the fused glasses were analyzed using an inductively coupled plasma emission spectrometer (ICP-OES, PE 5300V). The analytical errors are  $<1\%$ . For the trace element analysis, the weighed powdered samples were placed in a polytetrafluoroethylene (PTFE) pot, with the volume mixed acids of  $\text{HNO}_3 + \text{HClO}_4 + \text{HF}$  (1 + 1 + 2). Afterwards, the mixture was heated on a temperature-controlled electric hot plate, evaporated to dryness, and diluted to a constant volume. Finally, the samples were analyzed using an inductively coupled plasma mass spectrometer (ICP-MS, Agilent 7700). The US Geological Survey standards (AGV-2, BHVO-2, BCR-2, RGM2) showed that the error of most trace elements was less than 5%, and the error of the analysis of some volatile elements and very-low-content elements was less than 10%. The specific sample digestion procedure and ICP-MS determination method were referred to in [45].

##### 4.2. Zircon U-Pb Dating

The samples were crushed to 100 mesh. Representative zircon grains were hand-picked under binoculars and prepared into epoxy resin sample targets. The zircons were photographed using a polarization optical microscope with transmitted and reflected light and then carbon-coated. Cathodoluminescence (CL) photography was performed on the coated sample targets using scanning electron microscopy. Zircon documentation was performed at YuHeng Rock and Mineral Technology Service Co. in Hebei Province (China). LA-ICP-MS U-Pb zircon dating was performed in the Tianjin Geological Survey Center of the China Geological Survey. The instrument used was an Agilent 7900 coupled with

a RESOLUTION LR 193 nm ArF excimer laser system. Helium was applied as a carrier gas, and Ar was used as the make-up gas and mixed with the carrier gas via a T-connector before entering the ICP source. Nitrogen was added to the central-gas flow (Ar + He) of the Ar plasma to lower the detection limits and improve precision. The size of the laser ablation spot was 29  $\mu\text{m}$ , the ablation frequency was 7 Hz, and the laser energy density was 3 J/cm<sup>2</sup>. The detailed operating conditions for the laser system and ICP-MS instrument are as described in [46]. For U-Pb isotope dating and trace element analysis, zircon 91500 and silicate glass NIST SRM 610 were used as external standards for the fractionation correction of the isotopes and trace elements. The Plesovice zircon was used as a standard sample to monitor the data quality. During the test, each measurement involved a 15 s blank signal and 50 s sample signal, and the raw data reduction was carried out using ICP MS Data Cal software [47]. The U-Pb age diagram and the calculation of the weighted average of the obtained ages were computed using Isoplot [48].

#### 4.3. Zircon Lu-Hf Isotopes

In situ LA-ICP-MS zircon Lu-Hf isotope analysis was accompanied by the zircon U-Pb isotope dating, where the Lu-Hf and U-Pb isotope ablation craters are located adjacent to each other in the same zircon grain and/or on the same growth zone. In situ zircon Hf isotope analysis was performed using a laser ablation inductively coupled plasma mass spectrometer (LA-ICP-MS) (NEPTUNE, Thermo Fisher, Waltham, MA, USA) and an argon fluoride excimer laser (NEW WAVE 193 nm FX, ESI, USA) in the experimental test room of the Tianjin Geological Survey Center of the China Geological Survey. In this test, helium was used as the carrier gas to transport the ablated sample from the ablation chamber to the ICP MS torch. The laser beam spot size was 50  $\mu\text{m}$ , the laser ablation time was 26 s, and the laser pulse frequency was 10 Hz. Zircon 91500, GJ-1, Mud Tank, and Temora were used as reference standards. The specific test steps and calibration methods are listed [49].

## 5. Results

### 5.1. Whole-Rock Geochemistry

The geochemical analyses of the Nanpo intrusive rocks are summarized in Supplementary Table S1. The SiO<sub>2</sub> contents of the diorite samples range between 60.72 wt% and 63.03 wt%. In the TAS diagram and QAP diagram (Figure 4a,b), the samples plot in the diorite area. The samples have high Al<sub>2</sub>O<sub>3</sub> (15.97–18.87 wt%), intermediate K<sub>2</sub>O (1.54–2.01 wt%), and high CaO contents (5.88–6.39 wt%). The total alkali (Na<sub>2</sub>O + K<sub>2</sub>O) contents range between 5.29 and 5.84 wt%, the Na<sub>2</sub>O/K<sub>2</sub>O value is 2.21–2.51, and the rock is relatively rich in sodium (3.34–4.51 wt%).

Due to the lower SiO<sub>2</sub> contents (56.26–57.60 wt%), the monzodiorite samples plot in the monzodiorite fields of the TAS and QAP diagrams (Figure 4a,b). The samples have the highest Al<sub>2</sub>O<sub>3</sub> (17.62–18.87 wt%) and K<sub>2</sub>O contents (1.75–2.37 wt%) among the three studied rock types. The granodiorites have the highest SiO<sub>2</sub> (63.22–65.95 wt%), the lowest Al<sub>2</sub>O<sub>3</sub> (15.97–16.82 wt%), and intermediate K<sub>2</sub>O (1.53–1.84 wt%) contents. The TiO<sub>2</sub> (0.40–0.53 wt%), P<sub>2</sub>O<sub>5</sub> (0.14–0.18 wt%), and TFe<sub>2</sub>O<sub>3</sub> (3.45–4.38 wt%) contents are low, and the samples plotted in the granodiorite fields in the TAS and QAP diagrams (Figure 4a,b). In general, the plutonic rock types (diorite, monzodiorite, and granodiorite) of the three lithological zones of the Nanpo diorite intrusive rocks have moderate SiO<sub>2</sub> (56.26–65.60 wt%), high Al<sub>2</sub>O<sub>3</sub> (15.97–18.97 wt%), and high Na<sub>2</sub>O (3.24–5.00 wt%) contents, and all show intermediate Mg# values (42–50). In addition, the samples' Rittmann indexes  $\sigma$  are low (1.12–3.73), and they generally exhibit the properties of medium–high potassium metaluminous series calc-alkaline rocks (Figure 4c,d).

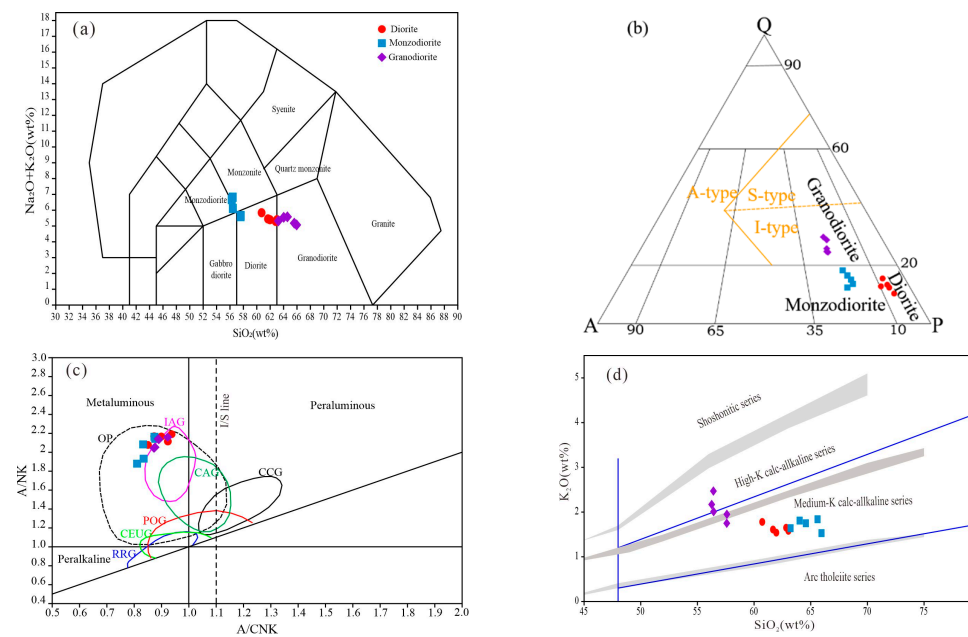


**Figure 4.** Major element diagrams of the Nanpo diorite pluton. (a) Total alkali versus silica diagram [50]; (b) QAP normative composition diagram [51] for the classification of the Nanpo diorite pluton; (c) A/NK vs. A/CNK diagram after [51]; (d) SiO<sub>2</sub> vs. K<sub>2</sub>O diagram [52]. Abbreviations: IAG—Island arc granitoids, CAG—Continental arc granitoids, CCG—Continental collision granitoids, POG—Post-orogenic granitoids, RRG—Granitoids related to rifts, CEUG—Granitoids related to continental uplift, OP—Oceanic plagioclase granite.

The trace and rare earth element characteristics of the Nanpo diorite intrusive rocks are remarkably similar. All rock types show low total rare earth element contents, with  $\Sigma$ REE ranging from 101 to 174 ppm (with a mean value of 140 ppm ( $n = 15$ )),  $\delta$ Eu values of 0.74–1.24 (with a mean value of 0.91 ( $n = 15$ )), and a weak Eu negative anomaly. LREE/HREE ratios of 6.14–11.01 (mean value of 7.88 ( $n = 15$ )) indicate enrichment in light rare earth elements (LREEs) and depletion in heavy rare earth elements (HREEs, Figure 5a). The values of  $(La/Yb)_N$  range from 6.96 to 13.80, with the average value of 8.6 ( $n = 15$ ), showing the fractionation of light and heavy rare earth elements. The  $(La/Sm)_N$  values of 2.97–7.61 indicate the strong fractionation of light rare earth elements, whereas  $(Gd/Yb)_N$  ratios of 1.20–1.69 record the weak fractionation of heavy rare earth elements. The standardized spidergram normalized to the primitive mantle (Figure 5b) documents the enrichment of the large ionic lithophile elements, including Rb, Ba, Th, K, and Sr, and the significant depletion of the high field strength elements, such as Nb, P, and Ti. The geochemical characteristics are diagnostic of plutonic rocks from island arcs [53,54].

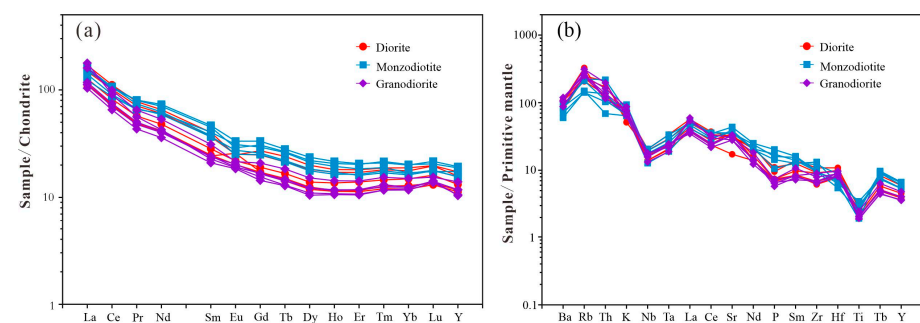


**Figure 5.** (a) Chondrite-normalized REE distribution patterns and (b) Primitive mantle-normalized incompatible element distribution patterns of the Nanpo diorite pluton. Normalization values are taken from [53,54].

### 5.2. Zircon U-Pb Dating

A total of 27 spot analyses on zircon from the diorite sample NP01-2 show  $^{206}\text{Pb}/^{238}\text{U}$  ages between  $189 \pm 2$  Ma and  $259 \pm 3$  Ma in Supplementary Table S2. The 16 analytical points that are concentrated on and near the Concordia yield a weighted average age of  $249.0 \pm 2.4$  Ma (Figure 6a,b). The 24 spot analyses of zircon from the monzodiorite sample NP13-5 yield ages between  $240 \pm 2$  and  $256 \pm 3$  Ma in Supplementary Table S2. All analyses are concentrated on and near Concordia. The concordant analyses define a weighted average age of  $247.0 \pm 2$  Ma (Figure 6c). A total of 24 spot analyses of zircon grains of granodiorite (NP 23-1) range between the ages of  $240 \pm 2$  and  $256 \pm 3$  Ma in Supplementary Table S2. All analyses are concordant. The concordant analyses yield a weighted average age of  $247.9 \pm 1.0$  Ma (Figure 6d). The U content ranged between 127 and 1406 ppm, with a mean value of 468 ppm. Therefore, the U-Pb age determined in our study is not affected by high U contents (2500 ppm) [55].

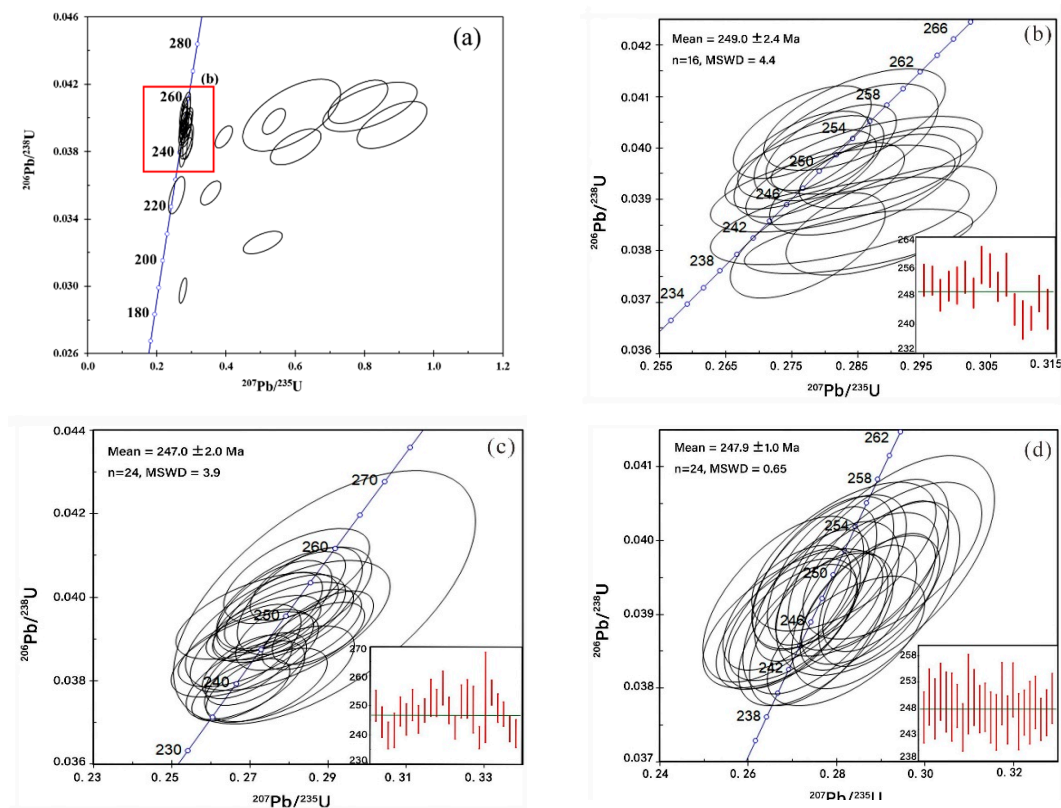


**Figure 6.** Zircon U-Pb age Concordia diagram and weighted average diagram of the Nanpo diorite pluton. (a,b) NP01-2 diorite; (c) NP13-5 monzodiorite; (d) NP 23-1 granodiorite.

### 5.3. Zircon Lu-Hf Isotopes

Zircon Lu-Hf isotopic analyses of the Nanpo diorite intrusive rocks are shown in Supplementary Table S3. Twenty-seven spots were analyzed for the sample NP01-2, and all the analyses have similar initial  $^{176}\text{Hf}/^{177}\text{Hf}$  values between 0.000974 and 0.002768. The  $\epsilon\text{Hf}(t)$  values are between  $+8.3 \sim +12$ , and the corresponding Hf isotope crustal model ages ( $T_{\text{DM}2}$ ) range from 513 to 726 Ma (Figure 7a,b). The  $^{176}\text{Hf}/^{177}\text{Hf}$  values of 24 spots of monzodiorite (sample NP13-5) are 0.000718~0.001593, the  $\epsilon\text{Hf}(t)$  values are between  $+6.7$  and  $+10.9$ , and the corresponding Hf isotope crustal model ages ( $T_{\text{DM}2}$ ) range from 573 Ma to 845 Ma (Figure 7c,d). The granodiorite (sample NP23-1) has  $^{176}\text{Hf}/^{177}\text{Hf}$  values ranging from 0.000718 to 0.001593 and  $\epsilon\text{Hf}(t)$  values between  $+6.7$  and  $+11.9$  for 24 spots, corresponding to Hf isotopic crustal model ages ( $T_{\text{DM}2}$ ) ranging from 512 Ma to 843 Ma (Figure 7e,f).

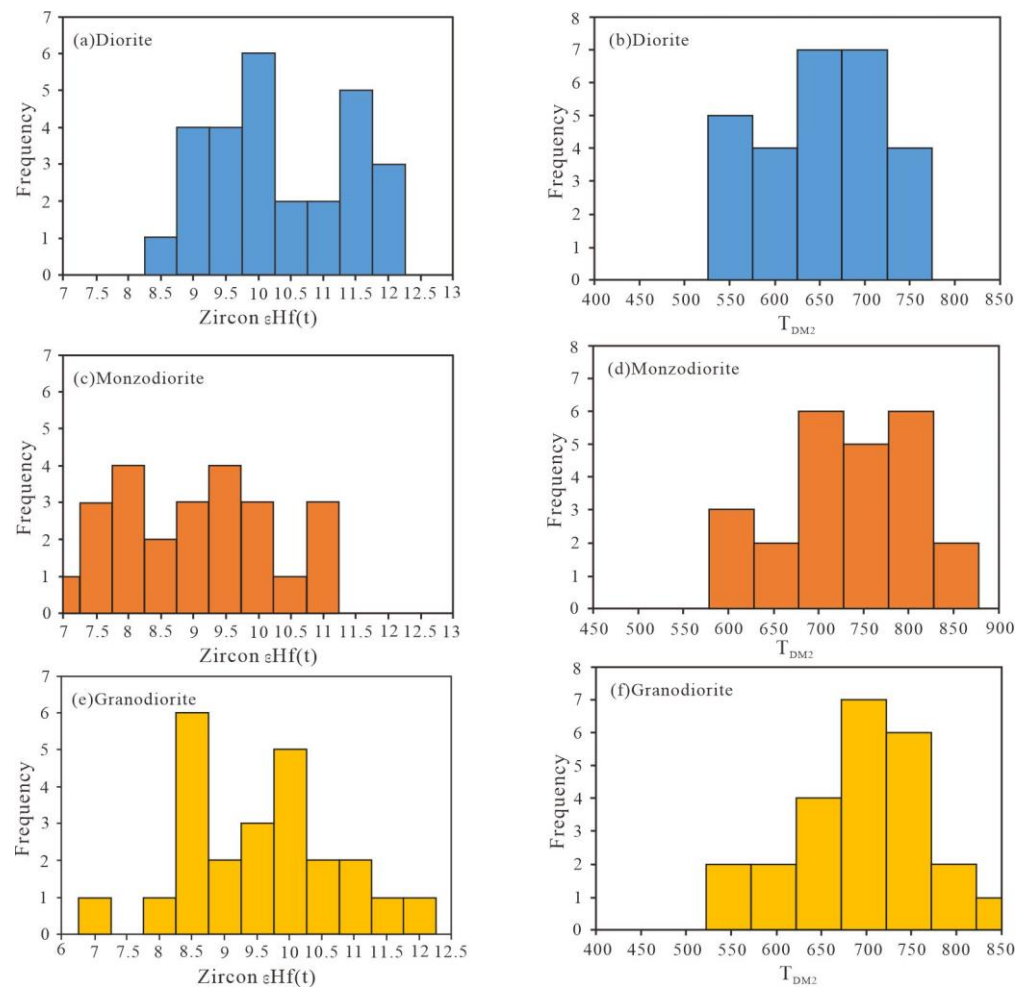


**Figure 7.** Distribution of zircon  $\epsilon\text{Hf}(t)$  values and Hf model ages of the Nanpo diorite pluton. (a,b) NP01-2 diorite; (c,d) NP13-5 monzogranite; (e,f) NP 23-1 granodiorite.

## 6. Discussion

### 6.1. Petrogenesis

Adakitic rocks were originally discovered by Defant and Drummond [26] in the Adak Island arc of the Cenozoic Aleutian Islands (USA) and are volcanic or intrusive rocks with specific geochemical characteristics. The formation of these rocks is related to the subduction of relatively young ( $\leq 25$  Ma) oceanic crust [26]. Plutonic adakites generally exhibit moderate  $\text{SiO}_2$  ( $\geq 56$  wt%), high  $\text{Al}_2\text{O}_3$  ( $\geq 15$  wt%), low  $\text{MgO}$  ( $< 3$  wt%), and high Sr ( $> 400$  ppm) contents. In addition, they have low heavy rare earth contents and high Sr/Y and La/Yb ratios, with no or weakly negative Eu anomalies, which are usually considered to be related to the source area of the magma [28].

The petrogenesis of the adakites has become a research hotspot in recent years. Several models are currently discussed: (1) partial melting of the demineralized lower crust, (2) slab dehydration/partial melting during the subduction of oceanic crust, (3) partial melting of thickened basaltic lower crust, (4) high-pressure fractional crystallization (involving garnet) of mafic magmas, (5) mixing of basaltic and feldspathic magma, and (6) assimilation-fractional crystallization (AFC) processes and differentiation of basaltic magma [56–60]. Therefore, identifying the genetic types of adakites is the key to revealing the tectonic magmatic evolution history and crustal growth mechanism of the ancient orogenic belt.

Petrological characteristics, similar geochemical characteristics, and almost identical zircon U-Pb ages indicate that the three recognized lithological zones in the Nanpo intrusive body are contemporaneous products of the in situ differentiation of an everyday parental

melt. This study found that Nanpo diorite intrusive rock has adakite affinity, including intermediate  $\text{SiO}_2$  (56.26–65.60 wt%), high  $\text{Al}_2\text{O}_3$  (15.97–18.97 wt%), high  $\text{Na}_2\text{O}$  (3.24–5.00 wt%), and high Sr (590–918 ppm) content, low Y (6.30–11.89 ppm) and Yb (1.99–3.44 ppm) contents, and high Sr/Y and La/Yb ratios, resembling the composition of adakitic rocks [26]. In the  $(\text{La}/\text{Yb})_N$ – $(\text{Yb})_N$  and Sr/Y–Y diagrams (Figure 8a,b), all of the studied samples were plotted in the field of adakite rock, which corroborates this interpretation.

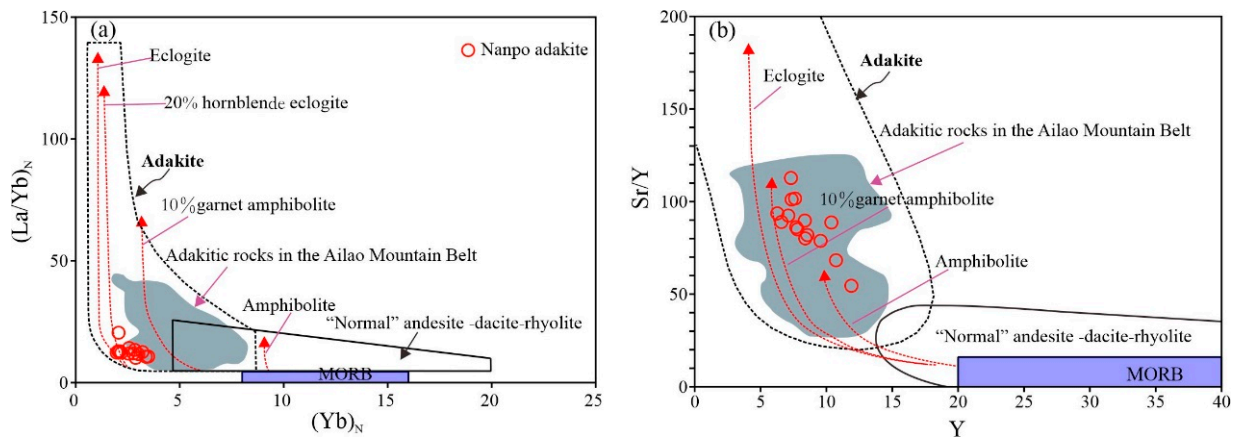


**Figure 8.** (a)  $(\text{La}/\text{Yb})_N$  versus  $(\text{Yb})_N$  and (b) Sr/Y versus Y diagrams for the studied adakitic rocks [26,36]; the data of adakitic rocks in the Ailao Mountain belt are from [61].

Whether it is the delamination of the lower crust or the melting of the subducted oceanic crust plate itself, the adakite itself will interact with the overlying mantle peridotite, which will inevitably lead to the increase in MgO (or Mg# value > 60) and incompatible elements such as Co, Cr, and Ni [36]. The Nanpo diorite rocks have moderate Mg# values (42–50), low MgO values (1.28–2.63 wt%), and low–moderate contents of incompatible elements, such as Co (3.98–20.30 ppm), Cr (24.50–47.83 ppm), and Ni (3.76–10.44 ppm). The data indicate that the magma forming the rock mass is not derived from the partial melting of the delaminated lower crust or subducted oceanic crust plate. The Nanpo adakitic diorite rock is not likely to have formed via basaltic slab melting since the examined adakitic rocks exhibit weak juvenile zircon Hf isotopes ( $\text{Hf}(t) = 1.80\text{--}4.03$ ), which are substantially lower than the Paleo-Tethyan MORB ( $\text{Hf}(t) = 15\text{--}20$ ) [36]. Additionally, experimental studies and phase equilibrium modeling show that the melting of either pristine or changed oceanic basaltic slab typically results in the production of high- $\text{SiO}_2$  and strongly sodic adakitic melts [27]. The examined Nanpo adakitic rocks, however, have low levels of  $\text{Al}_2\text{O}_3$  (15.97%–18.97% wt%) and moderate contents of  $\text{SiO}_2$  (56.26%–65.60% wt%) and MgO (1.28–2.63 wt%), in contrast to the melts, which are typically rich in  $\text{SiO}_2$  (>68 wt%) and  $\text{Al}_2\text{O}_3$  (>18 wt%) but poor in MgO (<0.2 wt%).

In general, adakite magmas derived from the partial melting of the thickened basaltic lower crust without crust–mantle interaction have a relatively low MgO content and Mg# values. These melts typically have low Mg# values (<40), regardless of the degree of melting [31]. However, the Nanpo adakitic diorite rocks have a moderate MgO content and moderate Mg# values (MgO = 1.28–2.63 wt%; Mg# = 42–50), which are different from the adakitic rocks formed by the partial melting of the thickened basaltic lower crust. Adakites formed by the high-pressure segregation crystallization of Mg-Fe magmas usually have relatively high  $(\text{Gd}/\text{Yb})_N$  ratios (>5.8) [62]. However, the Nanpo adakites exhibit significantly lower  $(\text{Gd}/\text{Yb})_N$  values (1.20–1.69). As the Nanpo adakites show a partial melting trend rather than a partial crystallization trend (Figure 9a), their formation through the fractional crystallization of basaltic magma is excluded. This is because the Nanjing adakite is distinct from the typical adakite produced by the fractional crystallization of basalt magma, which typically has a low  $\text{SiO}_2$  content [62,63]. In addition, considering that high-pressure fractional crystallization involving garnet usually leads to a decrease

in HREE and Y contents, the Sr/Y ratio in the residual magma should increase with the increase in the MgO content [63,64]. However, in the Sr/Y and MgO diagrams, the Nanpo adakites do not show this trend (Figure 9b). In addition, adakitic rocks produced by basaltic magma assimilation and fractional crystallization (AFC process) usually require large volumes of basalt-dacite rocks [63,64]. Therefore, the lack of co-magmatic mafic rocks, mixed structures, and mafic enclaves in the study area excludes the formation of the adakites through AFC processes from basaltic magma.

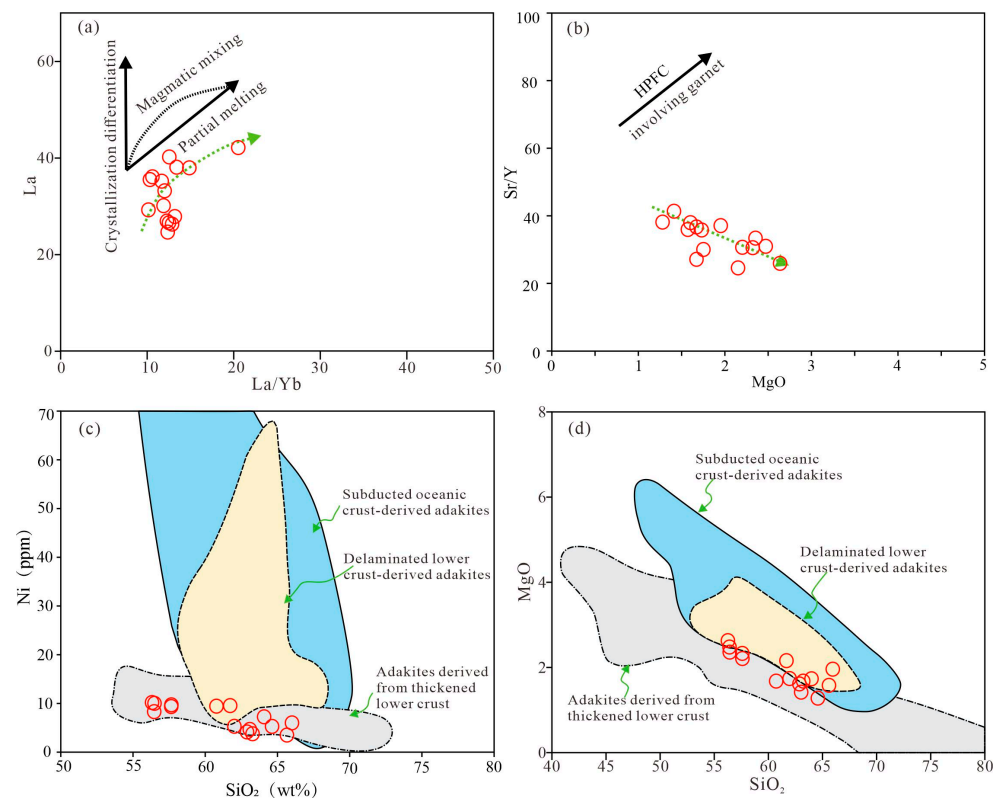


**Figure 9.** Genetic discrimination diagram of the Nanpo diorite intrusive rocks. (a) La versus La/Yb and (b) Sr/Y versus MgO diagrams are from [65]; (c) Ni versus SiO<sub>2</sub> and (d) MgO versus SiO<sub>2</sub> diagrams are from [66,67]. HPFC = high-pressure fractional crystallization.

The adakites of Nanpo have ancient zircon Hf isotopic model ages (512–845 Ma). Their low Na<sub>2</sub>O/K<sub>2</sub>O ratios (1.75–2.51) and calc-alkaline affinity (Figure 4d) are similar to the composition of felsic rocks formed by the partial melting of the ancient lower crust in the Paleo-Tethys tectonic domain [44]. The Nanpo rocks belong to the metaluminous series, with a striking negative P and Ti anomaly, suggesting that their source area is dominated by crust-derived material, which is also supported by SiO<sub>2</sub>-Ni and SiO<sub>2</sub>-MgO diagrams (Figure 9c,d). We propose that magma mixing between mantle-derived basaltic melt and crust-derived felsic magma is the most likely mechanism for the formation of Nanpo adakites. Their moderate SiO<sub>2</sub> contents (56.26–65.60 wt%), intermediate Mg# values (42–50), and low Hf isotope values support the crust–mantle interaction model. In the zircon age-εHf (t) correlation diagram (Figure 10), all the measuring points of the diorite intrusive rock are projected below the depleted mantle evolution line and above the chondrite evolution line and are closer to the depleted mantle evolution line, indicating the important contribution of mantle-derived magma. In addition, these samples are enriched in light rare earth elements and large ion lithophile elements, such as Rb, Ba, Th, K, and Sr, and are depleted in high-field-strength elements, such as Nb, P, and Ti. Ratios of specific high-field-strength elements also support the crust–mantle mixing model. For example, their Ce/Pb ratios (4.89–13.09) and Rb/Sr ratios (0.1–0.34) are between the upper mantle

average ( $Ce/Pb = 25 \pm 5$ ;  $Rb/Sr = 0.034$ ) and the crustal average ( $Ce/Pb = 4$ ;  $Rb/Sr = 0.35$ ). Moreover, the zircon Hf isotope compositions show a wide variation in the  $\epsilon_{Hf}(t)$  values (6.7–12.0), also suggesting a mantle component. In addition, the relatively high Th/Yb ratio (2.01–8.0)  $> 2$  and the relatively low Nb/La ratio (0.22–0.50)  $< 1$  are additional striking indicators for a mixed crust–mantle source.

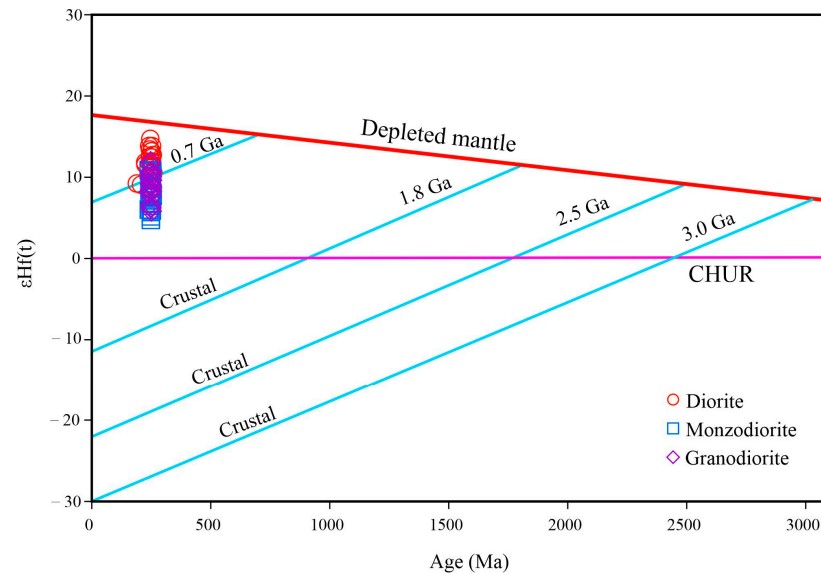


**Figure 10.** Age (Ma) vs.  $\epsilon_{Hf}(t)$  diagram of the Nanpo diorite pluton [56].

## 6.2. Tectonic Background and Geological Significance

The tectonic evolution of the Paleo-Tethys orogenic belt in Southeast Asia from the late Paleozoic to early Mesozoic is still controversial [68]. Previous studies have shown that the Southeast Asian region was the hinterland of back-arc basins and continental arcs in the late Carboniferous and late Triassic, respectively [2,21]. However, the timing of the tectonic transformation from oceanic plate subduction to continental collision in Southeast Asia and the physical and chemical response of the deep crust in the northwestern margin of the Indochina Block during the early collision phase have not been solved. Because of the striking coupling between the formation mechanism of adakite rocks and different tectonic settings [30], detailed petrogenetic studies can help to understand the tectonic evolution of the Late Paleozoic–Mesozoic Paleo-Tethys orogenic belt in Southeast Asia. Our discussion on their possible petrogenesis indicates that the adakitic melt in Nanpo is mainly derived from crust–mantle magma mixing and suggests that the early Triassic adakitic magma in the Luang Prabang–Loei tectonic belt comprises major contributions of mantle material. In addition, previous studies have documented at least four episodes of magmatic activity in the conversion process of the Luang Prabang–Loei tectonic belt from the Carboniferous back-arc basin to the Triassic continental arc setting. They were accompanied by multiple gold–silver–copper polymetallic mineralization [44]. The Middle–Late Permian–Early Triassic is the main metallogenic stage of porphyry/skarn-type Au–Ag deposits (e.g., PangKuang Au–Ag deposit and Phu Hin Lek Fai Cu–Au deposit) and epithermal Au–Ag deposits (e.g., Chatree Au–Ag deposit), indicating that Luang Prabang–Loei was in a special tectonic setting during this period [4,9,69].

The data document that the magmatic rocks of the Nanpo magmatic body intruded between 247 and 249 Ma, showing an average age of 248 Ma. The Nanpo intrusive body was formed as a result of early Triassic magmatic activity, as shown by the very small range of variation and the emplacement date of around 248 Ma. In addition, a  $189 \pm 2$  Ma old zircon in the diorite (NP01-2) suggests that the magmatism in the study area may have extended from the early Triassic to the early Jurassic. Based on our geochemical analysis of the Nanpo intrusive rocks, we propose that crust–mantle magma mixing is the

main formation mechanism of the Early Triassic adakite rocks in the Luang Prabang-Loei tectonic belt. Therefore, revealing the source of the Early Triassic mantle-derived magma is the key to understanding the tectonic setting of the Early Triassic adakite magmatism. Previous studies have shown that tectonic processes, such as mid-ocean ridge subduction, plate breakup, plate folding, and lithospheric destruction and sinking, may have induced the bottom intrusion of mantle-derived magma. This process can not only cause the vertical accretion of the crust (resulting in increased crustal thickness) but can also keep the lower crust in a high heat flow state. This, in turn, can induce subsequent partial melting of the crust and magma mixing, creating favorable conditions for the formation of adakites [17,70,71].

At present, no Triassic basaltic rocks with N-MORB affinity, intra-oceanic island arc magnesian-iron-rich lavas, or Permian-Triassic magmatic events with obvious temporal migration trends have been identified or reported in the Luang Prabang-Loei tectonic belt. Therefore, the model of mid-ocean ridge subduction and plate refolding has been excluded [3,11]. In addition, the associated magma formed by lithospheric disintegration would have interacted with mantle wedge peridotite to form adakitic magma with high Ni and Cr contents [2,27], inconsistent with the low Cr and Ni contents of the Nanpo adakites. The Nanpo adakites show a relative enrichment in LREE and large ion lithophile elements (Rb, Ba, K) and are deficient in high-field-strength elements (Nb, Ta, Ti). This is characteristic of subduction zone-related island arc magmatism. In addition, the high Zr contents (69–147 ppm) and La/Nb ratios (2.0–4.5) also reflect active continental margin arc magmatism. All samples plot in the field of a collisional setting in the tectonic discrimination diagram (Figure 11a). The majority of samples fall into the pre-plate collisional setting in the R1-R2 factor discrimination diagram (Figure 11b), and they thereafter transition to the post-plate collisional uplift setting. The results indicate that the Nanpo adakites were formed in island-arc to land-land collision transition or co-collision. The adakites formed from the melting of an ancient sedimentary source in the deep crust, thus reflecting the closure of the Paleo-Tethys Ocean Basin in the Luang Prabang-Loei area in the Late Permian–Early Triassic.

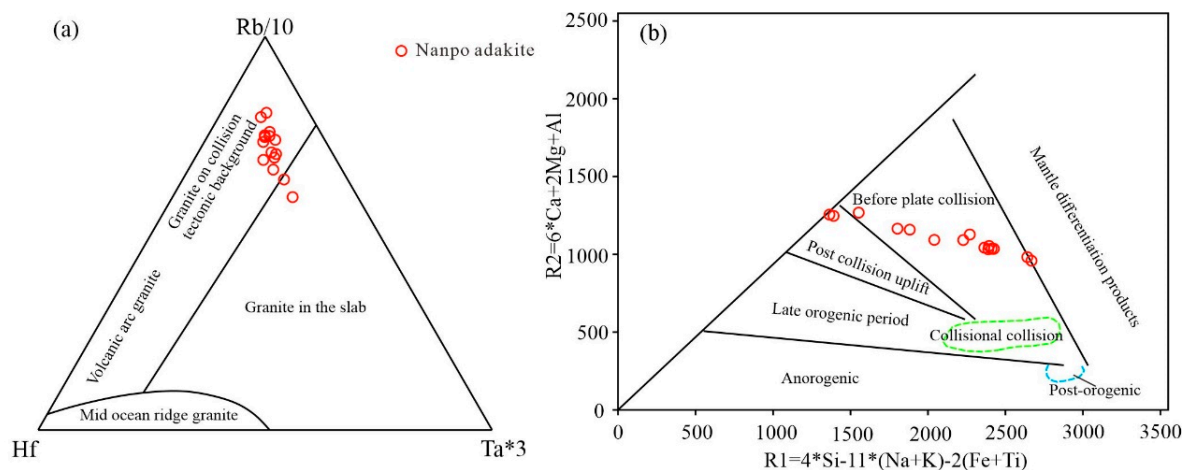


**Figure 11.** Discrimination diagram of the tectonic environment of the Nanpo adakitic diorite pluton. (a) Rb versus Hf versus Ta and (b) R1 versus R2 diagrams are from [72,73].

According to Villeneuve et al.'s [74] analysis of the Triassic sedimentary environment in Northern Vietnam's eastern Song Da and Sam Nua basins near the Indosinian Song Ma suture, the Paleo-Tethys branch of the Songma oceanic basin started subducting in the Permian and closed in the Middle Triassic. The study of bimodal volcanic rocks in the Jinshajiang–Ailaoshan–Song Ma orogenic belt also reveals that the Paleo-Tethys Ocean in Southeast Asia closed in the early Triassic and entered the post-collisional extensional environment in the middle-late Triassic [75]. Therefore, we propose that the closure of the

Paleo-Tethys Ocean Basin was accompanied by a plate fracture in the Luang Prabang-Loei tectonic zone during the Early Triassic, which led to the subduction of mantle-derived magnesian-iron-rich magma and facilitated the melting and subsequent magma mixing of the thickened crust (Figure 12). The plate fracture model also matches the linear distribution of the Late Paleozoic–Early Mesozoic island arc magmatism along the Paleo-Tethys suture zone in Southeast Asia. In addition, the intrusion of mantle-derived basaltic magma in the plate fracture model provides not only the heat but also mobilized valuable elements, such as Au-Ag-Cu, and may be the key factor for the formation of the Triassic mineralization in the Luang Prabang-Loei tectonic zone [76,77]. The Late Permian–Early Triassic terrestrial volcanic and sedimentary rocks (clastic and volcanic rocks) are overlying the marine and terrestrial strata (carbonate) in an angular unconformity, which also documents that the Luang Prabang-Loei tectonic belt entered a post-subduction collisional or extensional tectonic regime during this period [11].

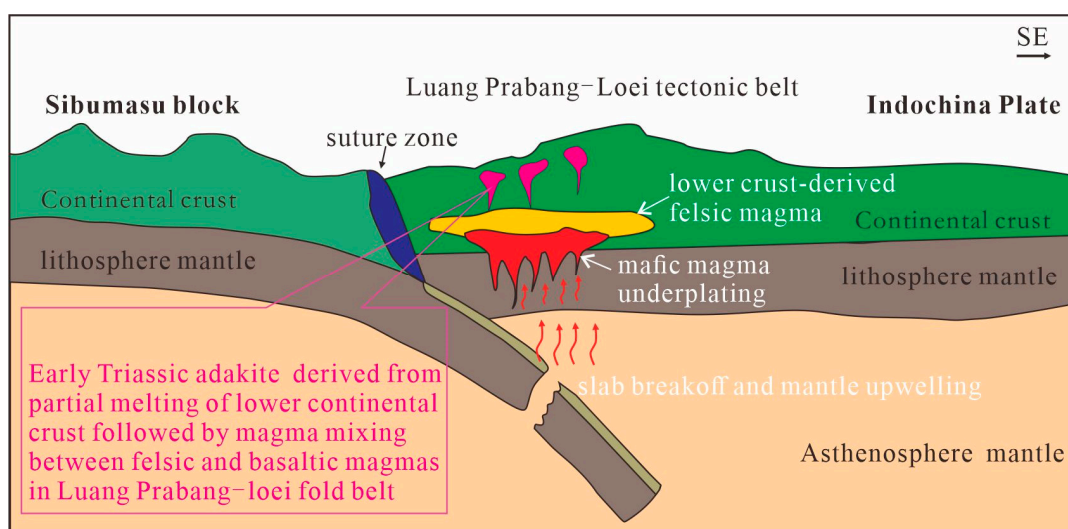


**Figure 12.** Tectonic evolution model of Early Triassic adakite magma in the Luang Prabang-Loei tectonic belt.

In recent years, different models for the generation of continental crust during the subduction, ablation, and collision of the Paleo-Tethys Ocean have been proposed. Some researchers have demonstrated that one key mechanism for the growth and evolution of the continental crust in the orogenic belt is the remelting of the ancient continental crust that was predominately composed of lithospheric mantle material and the addition of a small amount of mantle material [27,28]. Another key reason for the genesis of the orogenic belt, according to some researchers who have researched the early Mesozoic granites in the Central Asian orogenic belt, is the partial melting of the Paleo-Tethys oceanic crust or continental deposits during subduction [43].

The isotopic composition of the Triassic adakite in the Luang Prabang-Loei tectonic belt resembles rocks from the East Kunlun orogenic belt—the reworking of a dominantly ancient continental crust with a certain addition of lithospheric mantle materials. This conformity suggests that the Luang Prabang-Loei tectonic belt and the East Kunlun tectonic belt share the same crustal evolution. Based on our petrogenetic model from the adakitic rocks in Nanpo, we propose that the Triassic adakitic magma in the Luang Prabang-Loei tectonic belt mainly originated from the remelting of ancient crustal materials. Melting was associated with striking crust–mantle magma mixing, possibly a common process for the origin of Triassic adakitic magma and the formation of continental crust in Southeast Asia.

## 7. Conclusions

- (1) LA-ICP-MS zircon U-Pb geochronology documents the Early Triassic formation age (247–249 Ma) of the Nanpo adakites in Laos. Their composition is characterized by high Si, Al, Na, and Sr contents, low K, Mg, and Y contents, and intermediate Mg# values (42–50) that are typical for adakitic rocks.
- (2) Petrology, geochemistry, and zircon Lu-Hf isotopes indicate that the parental melts of the Nanpo adakites were derived from the partial melting of the thickened lower crust in the plate fault environment, and the mantle-derived magma participated in the magmatic evolution process.
- (3) Our study shows that the generation of Early Triassic adakite magmatism in the Luang Prabang-Loei tectonic belt may have been a response to the tectonic transition from oceanic subduction to post-subduction extension. The transformation of the ancient continental crust and the subsequent crust–mantle magma mixing are the main mechanisms for the growth of continental crust in the Paleo-Tethys orogenic belt in Southeast Asia.
- (4) The Luang Prabang-Loei Paleo-Tethys ocean basin closed in the Late Permian–Early Triassic, and then the Sibumasu block collided with the Indochina block in the Middle-Late Triassic.

**Supplementary Materials:** The following supporting information can be downloaded at: <https://www.mdpi.com/article/10.3390/min13060821/s1>, Table S1: Major elements, trace and rare earth element data; Table S2: Zircon U-Pb isotopic Dating Results; Table S3: Lu-Hf isotope data for zircons.

**Author Contributions:** H.L., J.G. and Z.H. designed the project; H.L. and B.W. conducted the original literature reviews; Y.L. and W.J. conducted the field geological survey; H.L. and J.G. wrote and organized the paper, with a careful discussion and revision by Y.G. All authors have read and agreed to the published version of the manuscript.

**Funding:** This research project is jointly funded by the mineral resources risk exploration project of the Laos LiDu Mining Company ([2011]d3-03) and the Laos, Cambodia, and adjacent areas of mineral resources potential evaluation of China Geological Survey (12120114018701).

**Data Availability Statement:** We have included the data and information in the Supplementary Materials of this submission.

**Acknowledgments:** The authors are thankful for the support of Laos Dynamics Mining Co., Ltd. We also thank the geochemical exploration team and the seventh geological team of Sichuan Provincial Bureau of Geology and Mineral Resources for their field technical support.

**Conflicts of Interest:** The authors declare no conflict of interest.

## References

1. Goldfarb, R.J.; Taylor, R.D.; Collins, G.S.; Goryachev, N.A.; Orlandini, O.F. Phanerozoic continental growth and gold metallogeny of Asia. *Gondwana Res.* **2014**, *25*, 48–102. [[CrossRef](#)]
2. Qian, X.; Feng, Q.; Wang, Y.; Chonglakmani, C.; Monjai, D. Geochronological and geochemical constraints on the mafic rocks along the Luang Prabang zone: Carboniferous back-arc setting in northwest Laos. *Lithos* **2016**, *245*, 60–75. [[CrossRef](#)]
3. Qian, X.; Feng, Q.; Yang, W.; Wang, Y.; Chonglakmani, C.; Monjai, D. Arc-like volcanic rocks in NW Laos: Geochronological and geochemical constraints and their tectonic implications. *J. Asian Earth Sci.* **2015**, *98*, 342–357. [[CrossRef](#)]
4. Shusheng, L.; Yongfei, Y.; Linnan, G.; Zhimin, P.; Guitang, P. Tectonic characteristics and metallogeny in Southeast Asia. *Geol. China* **2018**, *45*, 863–889. (In Chinese with English abstract)
5. Deng, J.; Wang, Q. Gold mineralization in China: Metallogenic provinces, deposit types and tectonic framework. *Gondwana Res.* **2016**, *36*, 219–274. [[CrossRef](#)]
6. Gan, J.; Li, H.; He, Z.; Gan, Y.; Mu, J.; Liu, H.; Wang, L. Application and Significance of Geological, Geochemical, and Geophysical Methods in the Nanpo Gold Field in Laos. *Minerals* **2022**, *12*, 96. [[CrossRef](#)]
7. Goldfarb, R.J.; Baker, T.; Dubé, B.; Groves, D.I.; Gosselin, P. Distribution, Character, and Genesis of Gold Deposits in Metamorphic Terranes. In *One Hundredth Anniversary Volume*; Society of Economic Geologists: Tucson, AZ, USA, 2005.
8. Guo, L.; Hou, L.; Liu, S.; Nie, F. Rare Earth Elements Geochemistry and C–O Isotope Characteristics of Hydrothermal Calcites: Implications for Fluid-Rock Reaction and Ore-Forming Processes in the Phapon Gold Deposit, NW Laos. *Minerals* **2018**, *8*, 438. [[CrossRef](#)]

9. Hou, L.; Xiong, F.; Wang, W.; Guo, L.; Peng, H.; Ni, S.; Zhang, Q. Carboniferous-Triassic felsic igneous rocks and typical mineral deposits in the Truong Son orogenic belt, SE Asia: Implications for Paleo-Tethyan tectonic evolution and metallogeny. *Ore Geol. Rev.* **2019**, *112*, 103036. [[CrossRef](#)]
10. Han, S.; Wang, S.; Tang, Z.; Tan, K.; Duan, X.; He, H.; Feng, Z.; Xie, Y. Integrated geophysical exploration of the coupling of a concealed rock body and metallogenic structures—Ag-Pb-Zn mining area case study in Jilinbaolige, Inner Mongolia, China. *J. Appl. Geophys.* **2020**, *178*, 104048. [[CrossRef](#)]
11. Shi, M.; Khin, Z.; Liu, S.; Xu, B.; Meffre, S.; Cong, F.; Nie, F.; Peng, Z.; Wu, Z. Geochronology and petrogenesis of Carboniferous and Triassic volcanic rocks in NW Laos: Implications for the tectonic evolution of the Loei Fold Belt. *J. Asian Earth Sci.* **2021**, *208*, 104661. [[CrossRef](#)]
12. Zaw, K.; Meffre, S.; Lai, C.; Burrett, C.; Santosh, M.; Graham, I.; Manaka, T.; Salam, A.; Kamvong, T.; Cromie, P. Tectonics and metallogeny of mainland Southeast Asia—A review and contribution. *Gondwana Res.* **2014**, *26*, 5–30.
13. Qian, X.; Li, H.; Yu, X.; Zhang, Y.; Wang, Y. Permian-Triassic Magmatism Along the Truong Son Zone in SE Asia and its Paleotethyan Tectonic Implications. *Geotectonic. Metallogeni.* **2022**, *46*, 585–604. (In Chinese with English abstract)
14. Metcalfe, I. Gondwana dispersion and Asian accretion: Tectonic and palaeogeographic evolution of eastern Tethys. *J. Asian Earth Sci.* **2013**, *66*, 1–33. [[CrossRef](#)]
15. Metcalfe, I.; Crowley, J.L. Upper Permian and Lower Triassic conodonts, high-precision U-Pb zircon ages and the Permian-Triassic boundary in the Malay Peninsula. *J. Asian Earth Sci.* **2020**, *199*, 104403. [[CrossRef](#)]
16. Sone, M.; Metcalfe, I.; Chaodumrong, P. The Chanthaburi terrane of southeastern Thailand: Stratigraphic confirmation as a disrupted segment of the Sukhothai Arc. *J. Asian Earth Sci.* **2012**, *61*, 16–32. [[CrossRef](#)]
17. Wang, H.; Lin, F.; Li, X.; Shi, M. The division of tectonic units and tectonic evolution in Laos and its adjacent regions. *Geol. China* **2015**, *42*, 71–84. (In Chinese with English abstract)
18. Shifeng, W.; Yasi, M.; Chao, W.; Peisheng, Y. Paleotethyan evolution of the Indochina Block as deduced from granites in northern Laos. *Gondwana Res.* **2016**, *38*, 183–196.
19. Xu, W.; Liu, F.; Xu, W.; Wang, H.; Ji, L.; Wang, F.; Wang, D. Geochemical and Geochronological Constraints of Permian-Triassic Magmatism on Oceanic Subduction and Continental Collision during the Eastern Paleo-Tethyan Evolution. *Minerals* **2022**, *12*, 633. [[CrossRef](#)]
20. Qian, X.; Wang, Y.; Feng, Q.; Zi, J.; Zhang, Y.; Chonglakmani, C. Petrogenesis and tectonic implication of the Late Triassic post-collisional volcanic rocks in Chiang Khong, NW Thailand. *Lithos* **2016**, *248–251*, 418–431. [[CrossRef](#)]
21. Xu, J.; Xia, X.; Huang, C.; Cai, K.; Yin, C.; Lai, C. Changes of provenance of Permian and Triassic sedimentary rocks from the Ailaoshan suture zone (SW China) with implications for the closure of the eastern Paleotethys. *J. Asian Earth Sci.* **2019**, *170*, 234–248. [[CrossRef](#)]
22. Metcalfe, I.; Henderson, C.M.; Wakita, K. Lower Permian conodonts from Palaeo-Tethys Ocean Plate Stratigraphy in the Chiang Mai-Chiang Rai Suture Zone, northern Thailand. *Gondwana Res.* **2017**, *44*, 54–66. [[CrossRef](#)]
23. Salam, A.; Zaw, K.; Meffre, S.; Mcphie, J.; Lai, C.K. Geochemistry and geochronology of the Chatree epithermal gold–silver deposit: Implications for the tectonic setting of the Loei Fold Belt, central Thailand. *Gondwana Res.* **2014**, *26*, 198–217. [[CrossRef](#)]
24. Shi, M.; Lin, F.; Fan, W.; Deng, Q.; Cong, F.; Tran, M.; Zhu, H.; Wang, H. Zircon U–Pb ages and geochemistry of granitoids in the Truong Son terrane, Vietnam: Tectonic and metallogenic implications. *J. Asian Earth Sci.* **2015**, *101*, 101–120. [[CrossRef](#)]
25. Yang, W.; Yuejun, W.; Shubo, L.; Seagren, E.; Yuzhi, Z.; Peizhen, Z.; Xin, Q. Exhumation and landscape evolution in eastern south China since the Cretaceous; new insights from fission-track thermochronology. *J. Asian Earth Sci.* **2020**, *191*, 104239.
26. Defant, M.J.; Drummond, M.S. Derivation of some modern arc magmas by melting of young subducted lithosphere. *Nature* **1990**, *347*, 662–665. [[CrossRef](#)]
27. Gan, J.; Xiong, F.; Xiao, Q.; Wang, W.; Yan, D. Petrogenesis and Geodynamic Implications of Late Triassic Mogetong Adakitic Pluton in East Kunlun Orogen, Northern Tibet: Constraints from Zircon U–Pb–Hf Isotopes and Whole-Rock Geochemistry. *Front. Earth Sci.* **2022**, *10*, 208. [[CrossRef](#)]
28. Xiong, F.H.; Ma, C.Q.; Zhang, J.Y.; Liu, B.; Jiang, H.A. Reworking of old continental lithosphere: An important crustal evolution mechanism in orogenic belts, as evidenced by Triassic I-type granitoids in the East Kunlun orogen, Northern Tibetan Plateau. *J. Geol. Soc.* **2014**, *171*, 847–863. [[CrossRef](#)]
29. Zhaohua, L.; Shan, K.; Hongwei, C. Characteristics, petrogenesis and tectonic implications of adakite. *Geol. Bull. China* **2002**, *7*, 436–440. (In Chinese with English abstract)
30. Wang, Q.; Zhao, Z.; Xiong, X.; Xu, J. Melting of the underplated basaltic lower crust: Evidence from the Shaxi adakitic sodic quartz diorite-porphyrites, Anhui Province, China. *Geochimica* **2001**, *4*, 353–362. (In Chinese with English abstract)
31. Castillo, P.R. Adakite petrogenesis. *Lithos* **2012**, *134–135*, 304–316. [[CrossRef](#)]
32. Chung, S.; Liu, D.; Ji, J.; Chu, M.; Lee, H.; Wen, D.; Lo, C.; Lee, T.; Qian, Q.; Zhang, Q. Adakites from continental collision zones: Melting of thickened lower crust beneath southern Tibet. *Geology* **2003**, *11*, 1021–1024. [[CrossRef](#)]
33. Hou, L.; Liu, S.; Guo, L.; Xiong, F.; Li, C.; Shi, M.; Zhang, Q.; Xu, S.; Wu, S. Geology, Geochronology, and Hf Isotopic Composition of the Pha Lek Fe Deposit, Northern Laos: Implications for Early Permian Subduction-Related Skarn Fe Mineralization in the Truong Son Belt. *J. Earth Sci. China* **2019**, *30*, 109–120. [[CrossRef](#)]

34. Yu, S.; Zhang, J.; Li, S.; Santosh, M.; Li, Y.; Liu, Y.; Li, X.; Peng, Y.; Sun, D.; Wang, Z.; et al. TTG-Adakitic-Like (Tonalitic-Trondhjemitic) Magmas Resulting From Partial Melting of Metagabbro Under High-Pressure Condition During Continental Collision in the North Qaidam UHP Terrane, Western China. *Tectonics* **2019**, *38*, 791–822. [[CrossRef](#)]
35. Qin, J.; Lai, S.; Grapes, R.; Diwu, C.; Ju, Y.; Li, Y. Origin of Late Triassic high-Mg adakitic granitoid rocks from the Dongjiangkou area, Qinling orogen, central China: Implications for subduction of continental crust. *Lithos* **2010**, *120*, 347–367. [[CrossRef](#)]
36. Martin, H.; Smithies, R.H.; Rapp, R.; Moyen, J.F.; Champion, D. An overview of adakite, tonalite–trondhjemite–granodiorite (TTG), and sanukitoid: Relationships and some implications for crustal evolution. *Lithos* **2005**, *79*, 1–24. [[CrossRef](#)]
37. Wu, F.Y.; Li, X.H.; Zheng, Y.F.; Gao, S. Lu–Hf isotopic systematics and their applications in peteology. *Acta Petrologica Sinica* **2007**, *23*, 185–220. (In Chinese with English abstract)
38. Scherer, E.E.; Cameron, K.L.; Blichert-Toft, J. Lu–Hf garnet geochronology; closure temperature relative to the Sm–Nd system and the effects of trace mineral inclusions. *Geochim. Cosmochim. Acta* **2000**, *64*, 3413–3432. [[CrossRef](#)]
39. Bouvier, A.; Vervoort, J.D.; Patchett, P.J. The Lu–Hf and Sm–Nd isotopic composition of CHUR: Constraints from unequilibrated chondrites and implications for the bulk composition of terrestrial planets. *Earth Planet Sci. Lett.* **2008**, *273*, 48–57. [[CrossRef](#)]
40. Li, Z.; Liu, S.; Wu, Z.; Jing, Z.; You, S. Main results of regional geological mapping of 1:200,000 B.Khon sheet in Laos. *China Geol. Surv.* **2018**, *5*, 10. (In Chinese with English abstract)
41. Li, S.C.; Wang, H.T.; Li, G.; Wang, X.A.; Yang, X.P.; Zhao, Z.R. Northward plate subduction process of the Paleo-Asian Ocean in the middle part of the Central Asian Orogenic Belt: Evidence from adakites. *Acta Petrologica Sinica* **2020**, *36*, 2521–2536. (In Chinese with English abstract)
42. Zhang, Y.Y.; Liu, K.; Wang, Y.; Zhang, D.; Mo, X.X.; Deng, Y.F.; Yu, T.X.; Zhao, Z.N. Geological Significance of Late Permian Magmatic Rocks in the Middle Section of the Ailaoshan Orogenic Belt, SW China: Constraints from Petrology, Geochemistry and Geochronology. *Minerals* **2022**, *12*, 652. [[CrossRef](#)]
43. Li, S.; Wang, T.; Wilde, S.A.; Tong, Y. Evolution, source and tectonic significance of Early Mesozoic granitoid magmatism in the Central Asian Orogenic Belt (central segment). *Earth-Sci. Rev.* **2013**, *126*, 206–234. [[CrossRef](#)]
44. Guo, L.; Hou, L.; Liu, S.; Zhang, Q.; Xu, S.; Shi, M.; Zeng, X. Ore–fluid sources and genesis of Phapon gold deposit, Laos: Constraint from REE and C, O, S isotopic characteristics. *Miner. Depos.* **2019**, *38*, 233–250. (In Chinese with English abstract)
45. Liu, Y.; Hu, Z.; Gao, S.; Günther, D.; Xu, J.; Gao, C.; Chen, H. In situ analysis of major and trace elements of anhydrous minerals by LA-ICP-MS without applying an internal standard. *Chem. Geol.* **2008**, *257*, 34–43. [[CrossRef](#)]
46. Li, H.K.; Geng, J.Z.; Hao, S.; Zhang, Y.Q.; Li, H.M. Study on the determination of zircon U–Pb isotope age by laser ablation multi receiver plasma mass spectrometer (LA-MC-ICPMS). *Acta Mineralogica Sinica* **2009**, *29*, 600–601. (In Chinese)
47. Liu, Y.; Gao, S.; Hu, Z.; Gao, C.; Zong, K.; Wang, D. Continental and Oceanic Crust Recycling-induced Melt–Peridotite Interactions in the Trans-North China Orogen: U–Pb Dating, Hf Isotopes and Trace Elements in Zircons from Mantle Xenoliths. *J. Petrol.* **2010**, *51*, 537–571. [[CrossRef](#)]
48. Ludwig, K.R. *User’s Manual for Isoplot/Ex Version 3.00: A Geochronological Toolkit for Microsoft Excel, 4ed.*; Berkeley Geochronology Center, Special Publication: Berkeley, CA, USA, 2003.
49. Geng, J.Z.; Li, H.K.; Zhang, J.; Zhou, H.Y.; Li, H.M. Zircon Hf isotope analysis by means of LA-MC-ICP-MS. *Geol. Bull. China* **2011**, *30*, 1508–1513. (In Chinese with English abstract)
50. Middlemost, E.A.K. Naming materials in the magma/igneous rock system. *Earth-Sci. Rev.* **1994**, *37*, 215–224. [[CrossRef](#)]
51. Maniar, P.D.; Piccoli, P.M. Tectonic discrimination of granitoids. *Geol. Soc. Am. Bull.* **1989**, *101*, 635–643. [[CrossRef](#)]
52. Peccerillo, A.; Taylor, S.R. Geochemistry of eocene calc-alkaline volcanic rocks from the Kastamonu area, Northern Turkey. *Contrib. Mineral. Petr.* **1976**, *58*, 63–81. [[CrossRef](#)]
53. Taylor, S.R. *The Continental Crust: Its Composition and Evolution; An Examination of the Geochemical Record Preserved in Sedimentary Rocks*; Blackwell Scientific Publications: Oxford, UK, 1985; p. 312.
54. Sun, S.S.; McDonough, W.F. Chemical and isotopic systematics of oceanic basalts: Implications for mantle composition and processes. *Geol. Soc. Lond. Spec. Publ.* **1989**, *42*, 313–345. [[CrossRef](#)]
55. Iles, K.A.; Hergt, J.M.; Sircombe, K.N.; Woodhead, J.D.; Bodorkos, S.; Williams, I.S. Portrait of a reference material: Zircon production in the Middledale Gabbroic Diorite, Australia, and its implications for the TEMORA standard. *Chem. Geol.* **2015**, *402*, 140–152. [[CrossRef](#)]
56. Yang, J.; Wu, F.; Shao, J.; Wilde, S.; Xie, L.; Liu, X. Constraints on the timing of uplift of the Yanshan Fold and Thrust Belt, North China. *Earth Planet Sci. Lett.* **2006**, *246*, 336–352. [[CrossRef](#)]
57. Atherton, M.P.; Petford, N. Generation of sodium-rich magmas from newly underplated basaltic crust. *Nature* **1993**, *362*, 144–146. [[CrossRef](#)]
58. Castillo, P.R. Origin of the adakite-high-Nb basalt association and its implications for postsubduction magmatism in Baja California, Mexico. *Geol. Soc. Am. Bull.* **2008**, *120*, 451–462. [[CrossRef](#)]
59. Konopelko, D.; Seltmann, R.; Dolgoplova, A.; Safonova, I.; Glorie, S.; De Grave, J.; Sun, M. Adakite-like granitoids of Songkultau: A relic of juvenile Cambrian arc in Kyrgyz Tien Shan. *Geosci. Front.* **2021**, *12*, 147–160. [[CrossRef](#)]
60. Liu, J.L.; Song, Z.J.; Cao, S.Y.; Zhai, Y.F.; Wang, A.J.; Gao, L.; Xiu, Q.Y.; Cao, D.H. The dynamic setting and processes of tectonic and magmatic evolution of the oblique collision zone between Indian and Eurasian plates: Exemplified by the tectonic evolution of the Three River region, eastern Tibet. *Acta Petrol. Sin.* **2006**, *22*, 775–786. (In Chinese with English abstract)

61. Lu, Y.J.; Kerrich, R.; Mccuaig, T.C.; Li, Z.X.; Hart, C.J.R.; Cawood, P.A.; Hou, Z.Q.; Bagas, L.; Cliff, J.; Belousova, E.A.; et al. Geochemical, Sr-Nd-Pb, and Zircon Hf-O Isotopic Compositions of Eocene-Oligocene Shoshonitic and Potassic Adakite-like Felsic Intrusions in Western Yunnan, SW China: Petrogenesis and Tectonic Implications. *J. Petrol.* **2013**, *54*, 1309–1348. [[CrossRef](#)]
62. Huang, F.; He, Y. Partial melting of the dry mafic continental crust: Implications for petrogenesis of C-type adakites. *Chin. Sci. Bull.* **2010**, *55*, 2428–2439. [[CrossRef](#)]
63. Laurent, O.; Doucelance, R.; Martin, H.; Moyen, J. Differentiation of the late-Archaean sanukitoid series and some implications for crustal growth: Insights from geochemical modelling on the Bulai pluton, Central Limpopo Belt, South Africa. *Precambrian Res.* **2013**, *227*, 186–203. [[CrossRef](#)]
64. Macpherson, C.G.; Dreher, S.T.; Thirlwall, M.F. Adakites without slab melting: High pressure differentiation of island arc magma, Mindanao, the Philippines. *Earth Planet Sci. Lett.* **2006**, *243*, 581–593. [[CrossRef](#)]
65. Drummond, M.S.; Defant, M.J.; Kepezhinskas, P.K. Petrogenesis of slab-derived trondhjemite-tonalite-dacite/adakite magmas. *Trans. R. Soc. Edinb. Earth Sci.* **1996**, *87*, 205–215.
66. WANG, Q.; XU, J.; JIAN, P.; BAO, Z.; ZHAO, Z.; LI, C.; XIONG, X.; MA, J. Petrogenesis of Adakitic Porphyries in an Extensional Tectonic Setting, Dexing, South China: Implications for the Genesis of Porphyry Copper Mineralization. *J. Petrol.* **2006**, *47*, 119–144. [[CrossRef](#)]
67. Chen, S.; Niu, Y.L.; Xue, Q.Q. Syn-collisional felsic magmatism and continental crust growth: A case study from the North Qilian Orogenic Belt at the northern margin of the Tibetan Plateau. *Lithos* **2018**, *308*, 53–64. [[CrossRef](#)]
68. Wu, S.; Nie, F.; Liu, S.; Xie, E.; Leng, Q.; Li, Y.; Wu, Z.; Zhang, H. The Discovery of Ophiolitic Complex in Namhonor, Northern Loei Tectonic Belt and Its Geological Significance. *Earth Sci.* **2022**, *47*, 2871–2888. (In Chinese with English abstract)
69. Shi, M.; Lin, F.; Li, X.; Ling, X.; Shi, H. Stratigraphic zoning and tectonic events in Indochina and adjacent areas of southwest China. *Geol. China* **2011**, *38*, 1244–1256. (In Chinese with English abstract)
70. Tang, M.; Ji, W.; Chu, X.; Wu, A.; Chen, C. Reconstructing crustal thickness evolution from europium anomalies in detrital zircons. *Geology* **2020**, *49*, 76–80. [[CrossRef](#)]
71. Wyllie, P.J. Volatile Components, Magmas, and Critical Fluids in Upwelling Mantle. *J. Petrol.* **2000**, *41*, 1195–1206. [[CrossRef](#)]
72. Harris, N.B.W.; Pearce, J.A.; Tindle, A.G. Geochemical characteristics of collision-zone magmatism. *Geol. Soc. Lond. Spec. Publ.* **2007**, *19*, 67–81. [[CrossRef](#)]
73. Batchelor, R.A.; Bowden, P. Petrogenetic interpretation of granitoid rock series using multicationic parameters. *Chem. Geol.* **1985**, *48*, 43–55. [[CrossRef](#)]
74. Villeneuve, M.; Rossignol, C.; Martini, R.; Cornée, J.; Bourquin, S. New insights into the Triassic sedimentary environment of the eastern parts of the Song Da and Sam Nua basins alongside the Indosinian Song Ma suture, Northern Vietnam. *J. Asian Earth Sci.* **2020**, *187*, 104067. [[CrossRef](#)]
75. Xu, J.; Xia, X.P.; Lai, C.; Long, X.; Huang, C. When Did the Paleotethys Ailaoshan Ocean Close: New Insights From Detrital Zircon U-Pb age and Hf Isotopes. *Tectonics* **2019**, *38*, 1798–1823. [[CrossRef](#)]
76. Chapman, J.B.; Ducea, M.N.; DeCelles, P.G.; Profeta, L. Tracking changes in crustal thickness during orogenic evolution with Sr/Y: an example from the North American Cordillera. *Geology* **2015**, *43*, 919–922. [[CrossRef](#)]
77. Li, G.J.; Wang, Q.F.; Yu, L.; Hu, Z.C.; Ma, N.; Huang, Y.H. Closure time of the Ailaoshan Paleo-Tethys Ocean: Constraints from the zircon U-Pb dating and geochemistry of the Late Permian granitoids. *Acta Petrol. Sin.* **2013**, *29*, 3883–3900. (In Chinese with English abstract)

**Disclaimer/Publisher’s Note:** The statements, opinions and data contained in all publications are solely those of the individual author(s) and contributor(s) and not of MDPI and/or the editor(s). MDPI and/or the editor(s) disclaim responsibility for any injury to people or property resulting from any ideas, methods, instructions or products referred to in the content.